MDPI

Article

Sliding Mode Input Current Control of the Synchronous DC-DC Buck Converter for Electro-Mechanical Actuator Emulation in More Electric Aircrafts

Mahdi Salimi [1,2,]*[ID], Christian Klumpner [2][ID] and Serhiy Bozhko [2]

[1] Faculty of Engineering and Science, University of Greenwich, Kent ME4 4TB, UK
[2] Power Electronics, Machines and Control (PEMC) Research Group, University of Nottingham, Nottingham NG7 2RD, UK
* Correspondence: m.salimi@gre.ac.uk

Publisher's Note: MDPI stays neutral with regard to jurisdictional claims in published maps and institutional affiliations.

Abstract: The main challenges of the input current control in synchronous DC-DC buck converters are the nonlinear model of the system, changes of the operating point in a wide range, and the need to use an input LC filter for current smoothing, which may result in the instability of the closed-loop system. In this paper, a step-by-step approach is developed for the design and improvement of a PI-feedforward closed-loop controller. It is shown that a linear PI controller cannot stabilize the closed-loop system properly during wide changes in model parameters, e.g., an equivalent series resistance of the input filter. To cope with the stability issues, a fixed-frequency sliding mode controller (SMC) has been developed in this paper for the implementation of an electro-mechanical actuator (EMA) emulator. Moreover, a systematic approach is proposed for controller tuning and the selection of the SMC's gains. To achieve high power efficiency, high-frequency GaN switches are used for the practical implementation of the DC-DC converter. Despite large changes in the load current, the designed nonlinear controller can track the input current reference satisfactorily. Steady-state and dynamic responses of the proposed SMC are compared with conventional linear controllers. Considering the Lyapunov stability theorem, it is proved that the designed SMC can stabilize the closed-loop system in the entire utilizable domain. The proposed nonlinear SMC controller enjoys a very simple control law. Hence, despite having very high switching and sampling frequencies, it can be easily implemented. The experimental response of the designed synchronous DC-DC buck converter is evaluated experimentally by implementing the control strategy in a TMS320F28335PGFA DSP from *Texas Instrument*. Moreover, the comprehensive comparison of the proposed SMC controller and a PI-feedforward controller proved the superior performance of the developed closed-loop system, in terms of the transient time response, robustness, and stability of the EMA emulator.

Keywords: EMA Emulator; SMC; input current control; synchronous DC-DC converters

1. Introduction

In order to address the high maintenance cost of non-electric actuators, more/all-electric aircraft that employ "power by wire" actuators are developed to replace them, and this trend has been rapidly increasing in recent years [1]. To drive the electric actuators in the aircraft, an efficient and light power converter that can control the currents and voltages very accurately and efficiently should be employed. The GaN semiconductor-based power switch is one of the most promising technologies in electric aircraft application, due to its extremely low switching loss [2]. By using the GaN power semiconductors, which facilitate the implementation of ultra-high-speed converters, the switching frequency can be increased up to several hundred kHz, which can reduce the converter's size and weight.

In Airbus A350 and A380, the wing flaps and slats of aircraft are controlled by electromechanical actuators (EMA). The fuel consumption reduction and ease of fault detection are the main advantages of the EMA, compared with the conventional hydraulic system.

For the reliable development and investigation of using novel EMAs in the aircraft power network, it is vital to be able to emulate the behaviour of the EMA by using a power converter-based emulator [3] for all ground testing of all future generation aircrafts.

In Figure 1, a typical profile for the current absorbed from the 270 V DC bus absorbed by a real EMA [4] and power topology of the developed EMA emulator are illustrated. To emulate the EMA system behaviour, it is necessary to implement a power converter that uses a DC-DC chopper configuration. It should be regulated with a current control loop to track any EMA current profile accurately, similar to the one illustrated in Figure 1a.

(a)

(b)
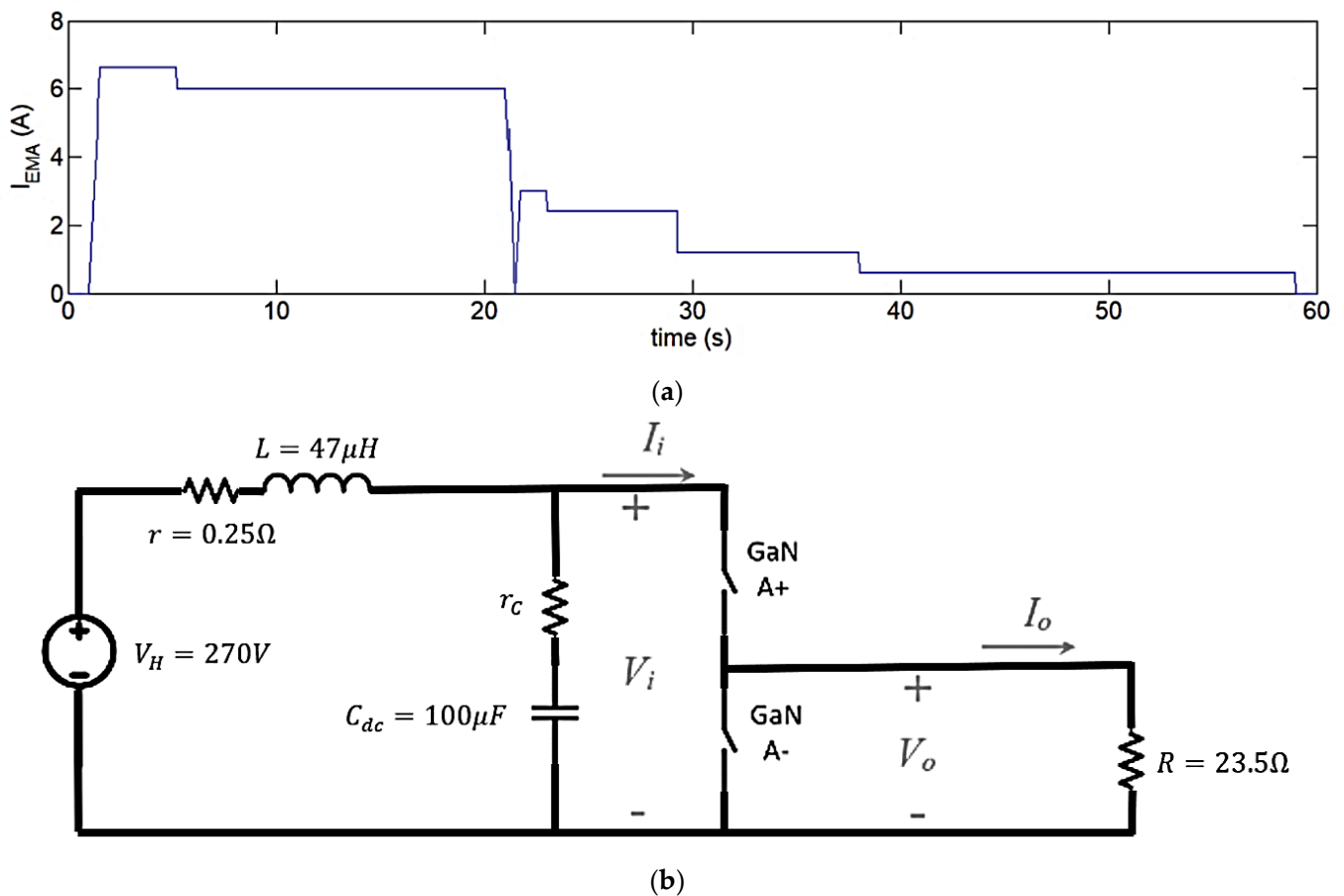
Figure 1. Typical profile of the current absorbed from 270V power bus by a real EMA [4] (**a**) and topology of the developed EMA emulator (**b**).

There are two main types of DC-DC converters, buck step-down and boost step-up choppers, that can be employed as an EMA emulator. From the controller design viewpoint, the DC-DC boost converter is a non-minimum phase system [5]. So, direct output voltage control of the boost DC-DC converter is a challenging task, due to the presence of a right half-plane zero in the system transfer function [5]. To cope with this problem, indirect output voltage controllers could be employed, which complicates the closed-loop system design and implementation [6]. Hence, in this paper, a DC-DC buck converter, which is a minimum phase system, will be studied as an EMA emulator, using the asynchronous step-down chopper [7].

In [8], the input current control of the DC-DC buck converter was studied for maximum power point tracking of the photovoltaic panels, and a detailed small-signal analysis of the photovoltaic-based battery charger was developed. To improve the accuracy of analysis, parasitic elements of the photovoltaic panel, including the source capacitance/inductance and interconnecting cable dynamics, were modelled. However, the linear controller was developed based on a small-signal approximation. It is well-known that the small-signal approximation can only model the system around the operating point, and it is not valid

on the entire range of the model changes. Hence, a linear controller cannot guarantee the stable and robust performance of a system in a wide range of operations.

On the other hand, model-based nonlinear controllers are designed based on the exact model of converter without the help of small-signal approximation. So, the operational domain of nonlinear controllers is not limited to the location of nominal operating point. For example, in [9], considering the passivity-based control, a nonlinear approach was developed for the closed-loop control of DC-DC converters. As a result, the asymptotic stability of the system can be maintained within the whole of the operating conditions. To decrease the number of required sensors, the state variables of the model were estimated based on the Hamiltonian framework. The asymptotic stability of designed closed-loop system was evaluated and proved using the Lyapunov theory. Due to the employment of an observer, the closed-loop controller can be implemented without input voltage and inductor current sensors. However, the observer's parameters are tuned by trial and error in [9]. Hence, the optimum functionality of closed-loop system cannot be guaranteed in [9].

As another example of a model-based nonlinear control method, the application of adaptive backstepping technique has been reported for closed-loop control of DC-DC converter in the presence of model nonlinearity and uncertainty [10]. The control law and parameter estimation rules are developed by adding the virtual control inputs successively into the Lyapunov function. Hence, adaptive backstepping can maintain the asymptotic stability of the system in a wide operating range, and its performance does not deteriorate by changes of the controlling gains. However, heavy calculations are needed for the implementation of an adaptive backstepping controller because, for each adaptation rule, a complex differential equation should be solved separately. For this reason, the adaptive backstepping controller is not a very good candidate for the closed-loop control of high-speed power electronics converters.

Moreover, an adaptive extremum-seeking approach for closed-loop control of the DC-DC buck converters was proposed in [11]. Utilizing a Lyapunov-based adaptive controller guarantees stability and robustness of the closed-loop system in a wide range of operations. For the practical implementation of the adaptive controllers, application of the powerful processors is mandatory for calculation of the control effort and estimation laws. In another word, the adaptive approach is not the first choice for real-time control of the power converters with GaN switches, which may operate at several hundred kHz. So, for closed-loop control of the EMA emulator, a nonlinear controller with a simple control law is a more interesting choice.

Considering the ease of implementation, fast transient response, and robustness in a wide range of operations, the application of sliding mode control (SMC) is a remarkable choice for the closed-loop control of the power converters. So, the SMC of the synchronous buck DC-DC converters is studied in [12]. To stabilize the switching frequency of the converter, an extra control-loop is needed for the adjustment of the hysteresis band of the SMC. The robustness of the developed controller is investigated at different operating points. However, as the input current of the standard DC-DC buck converter has a pulsating waveform, it cannot be employed for the EMA emulator directly. To smooth out the input current, an LC filter could be inserted between the voltage source and the input port of the buck choppers, as shown in Figure 1b. However, the existence of the LC filter may result in un-damped oscillations in the closed-loop system, which deteriorates the converter stability [13].

Briefly, the main challenges of the input current controller design for the EMA emulator can be summarized as follows:

(a)   Due to the nonlinear model of system, the use of conventional linear controllers is not straightforward. In this paper, although a modified PI-feedforward controller is developed analytically for the EMA emulator, it is seen that the controller cannot stabilize the closed-loop system against model uncertainty, e.g., changes in the input filter parameters.

(b) Changes of the operating point in a wide range. Considering the current profile of EMA in Figure 1a, the closed-loop controller needs to stabilize the system at different operating points. Hence, if the controller is tuned at a specific operating point using a small signal approximation, stability cannot be guaranteed within the whole operating domain.

(c) The application of an LC filter for current smoothing at the input port of EMA emulator complicates the controller design since the LC circuit has an inherent tendency to generate oscillation and instability.

To cope with these problems, a fixed-frequency SMC for the input current control of the DC-DC synchronous buck converter is designed in this paper, which can be employed as an EMA emulator. Despite the application of the LC input filter, the stability of the proposed controller is proved considering Lyapunov theory, so it can stabilize the closed-loop system in a wide range of operations. Moreover, a systematic approach is introduced for tuning the developed nonlinear controller and selection of the SMC's gains.

Moreover, the developed controller enjoys a simple control law. So, despite the fast switching of the GaN-based EMA emulator, the controller can be updated in each switching interval. It is shown that the proposed SMC has a superior transient response compared with conventional linear controllers. Using the TMS320F28335PGFA DSP from *Texas Instrument*, the experimental response of the designed synchronous DC-DC buck converter is evaluated as an EMA emulator. Despite the large changes of the load current, it is shown that the designed SMC is able to reject disturbances properly and stabilize the EMA current satisfactorily. Moreover, the comprehensive comparison of the proposed SMC controller and a PI-feedforward controller proved the superior performance of the developed closed-loop system, in terms of transient time response, robustness, and stability of EMA emulator.

2. Modelling of the EMA Converter

According to Figure 1b, in order to emulate the EMA in more electric aircraft, a synchronous chopper with resistive load (R) is employed. In the power topology, V_H is the input voltage that supplies the converter through a DC filter. The LC type filter is responsible for input current smoothing on the high voltage port of the converter.

Considering the PWM switching of the half-bridge converter, the equivalent input resistance, which is seen from the 270 V DC bus, can be calculated as follows:

$$R_i = \frac{V_i}{I_i} = \frac{\frac{V_0}{d}}{I_o} = \frac{\frac{V_o}{I_o}}{d} = \frac{R}{d} \tag{1}$$

where d is the averaged value of the duty-cycle and R is load resistance. So, $\frac{R}{d}$ is the equivalent impedance of the load resistor (R) that is transferred to the converter input port. In Figure 2, the averaged equivalent model of the converter is illustrated.

Considering $(x_1, x_2)^T = (i_{Ldc}, V_i)^T$ as a state vector of the system in Figure 2a, the averaged state-space model of the EMA emulator can be written as follows. It should be noted that in this equation, the parameter R refers to the load resistance.

$$\begin{pmatrix} \dot{x}_1 \\ \dot{x}_2 \end{pmatrix} = \begin{pmatrix} -\frac{r}{L_{dc}} & -\frac{1}{L_{dc}} \\ \frac{1}{C_{dc}} & -\frac{d}{RC_{dc}} \end{pmatrix} \begin{pmatrix} x_1 \\ x_2 \end{pmatrix} + \begin{pmatrix} \frac{V_H}{L_{dc}} \\ 0 \end{pmatrix} \tag{2}$$
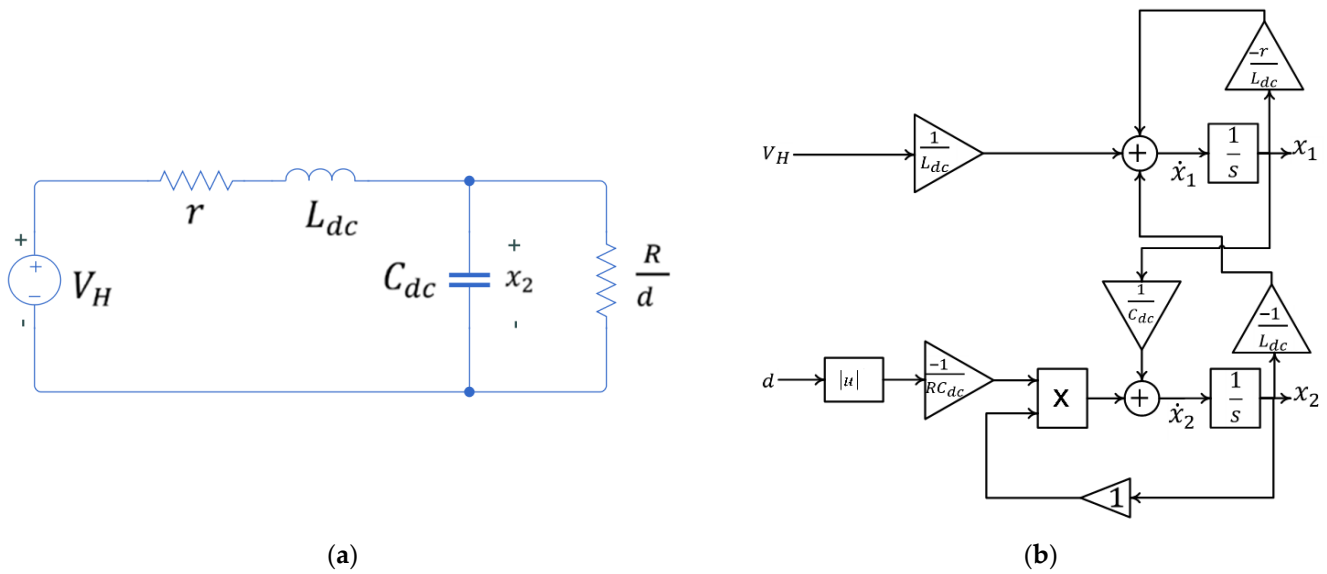
Figure 2. Averaged equivalent circuit (**a**) and dynamic model (**b**) of the EMA converter.

According to (2), dynamic model of the EMA emulator is illustrated in Figure 2b. It is seen that the EMA converter is a nonlinear system. Considering small-signal perturbations of the system:

$$d = D + \tilde{d} \tag{3}$$

$$x_1 = X_1 + \tilde{x}_1 \tag{4}$$

$$x_2 = X_2 + \tilde{x}_2 \tag{5}$$

where $\tilde{d}$, $\tilde{x}_1$, and $\tilde{x}_2$ are AC small perturbations of the parameters. Additionally, D, X_1, and X_2 are DC steady-state quantities. Using Equations (3)–(5) in Equation (2) and rearranging the DC and AC terms, the linearized averaged state-space model of the system can be obtained.

$$\begin{pmatrix} \dot{\tilde{x}}_1 \\ \dot{\tilde{x}}_2 \end{pmatrix} = \begin{pmatrix} -\frac{r}{L_{dc}} & -\frac{1}{L_{dc}} \\ \frac{1}{C_{dc}} & -\frac{D}{RC_{dc}} \end{pmatrix} \begin{pmatrix} \tilde{x}_1 \\ \tilde{x}_2 \end{pmatrix} + \begin{pmatrix} 0 \\ -\frac{DX_2}{RC_{dc}}\tilde{d} \end{pmatrix} \tag{6}$$

and steady-state model of the system can be written as:

$$\begin{pmatrix} \dot{X}_1 \\ \dot{X}_2 \end{pmatrix} = \begin{pmatrix} -\frac{r}{L_{dc}} & -\frac{1}{L_{dc}} \\ \frac{1}{C_{dc}} & -\frac{D}{RC_{dc}} \end{pmatrix} \begin{pmatrix} X_1 \\ X_2 \end{pmatrix} + \begin{pmatrix} \frac{V_H}{L_{dc}} \\ 0 \end{pmatrix} \tag{7}$$

Considering $\begin{pmatrix} \dot{X}_1 \\ \dot{X}_2 \end{pmatrix} = \begin{pmatrix} 0 \\ 0 \end{pmatrix}$ in Equation (7), the steady-state operating point of the EMA converter (X_{1s} and X_{2s}) can be calculated.

$$X_{1s} = \frac{D}{R} X_{2s} \tag{8}$$

$$X_{2s} = \frac{V_H}{1 + r\frac{D}{R}} \tag{9}$$

Applying Laplace transform to Equation (6) with zero initial conditions, small-signal transfer function (input current to duty-cycle) of the system can be written as:

$$H(s) = \frac{\tilde{x}_1}{\tilde{d}} = \frac{\frac{DX_2}{RC_{dc}}}{L_{dc}\left(s + \frac{D^2}{RC_{dc}}\right)\left(s + \frac{r}{L_{dc}}\right) + \frac{1}{C_{dc}}} \tag{10}$$

where D and X_2 are duty-cycle and capacitor voltage of the converter on the operating point.

3. Linear Controller

To control input current of the EMA emulator, block-diagram of the closed-loop system is shown in Figure 3. A linear PI controller is employed for regulation of the input current ($\tilde{x}_1$).
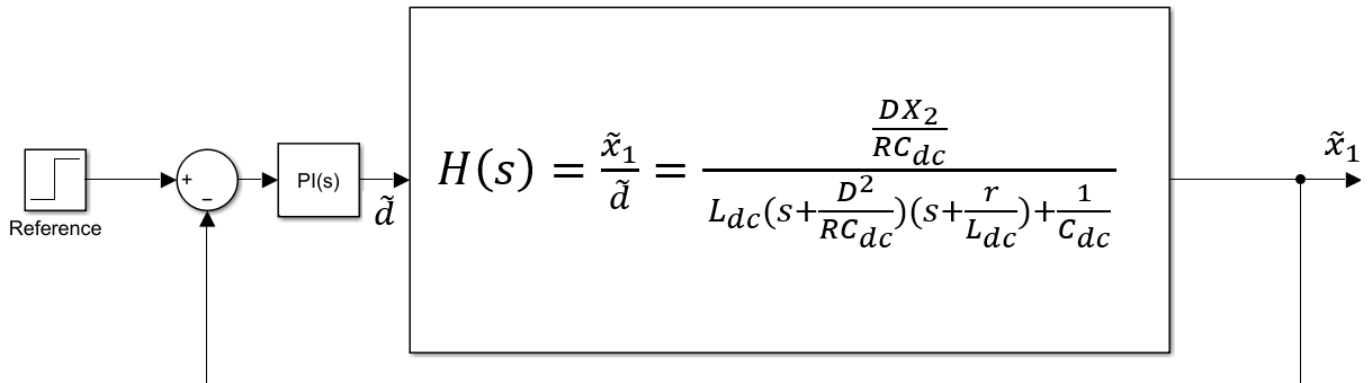
Figure 3. Linear closed-loop control of the EMA emulator.

Nominal values of the circuit components are given in Figure 1b. Assuming $X_{1s} = 1$ *Amper* as an operating point of the system, the capacitor voltage and duty-cycle of the converter can be calculated from (8) and (9) in the operating point as $X_{2s} = 269.9913$ V and $D = 0.087$. Hence, normalized transfer function of the system in (10) can be summarized as follows:

$$H(s) = \frac{4.25e8}{s^2 + 2.13e3 s + 2.12e8}$$

Gains of the controller (k_p and k_i) are tuned by using the MATLAB/Simulink toolbox in Table 1. To evaluate the response of the controller, the closed-loop system is simulated for step changes of the reference current from 1 A to 0 A in Figure 4. It is seen that rise/fall time of the linear controller is 10 ms.

Table 1. Details of the designed linear controller.

Controller Parameters	
	Tuned
P	0
I	109.417
D	—
N	—
Performance and Robustness	
	Tuned
Rise time	0.01 s
Settling time	0.0179 s
Overshoot	0%
Peak	1
Gain margin	19.8 dB
Phase margin	89.9 deg
Closed-loop Stability	stable
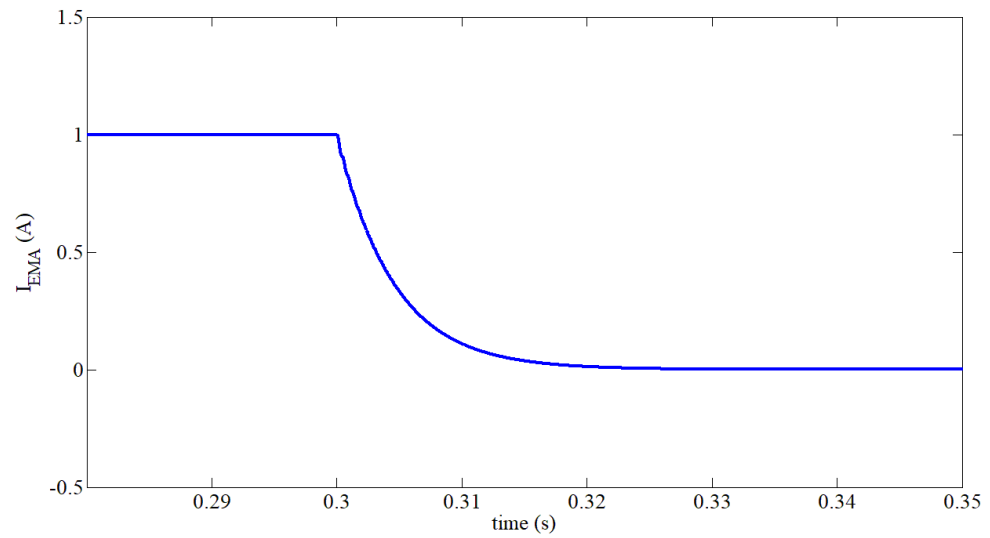
Figure 4. Response of the linear controller for step changes of the input current from 1 A to zero.

4. Stability Analysis of the Linear Controller

In the previous section, a PI controller is designed for current control of the EMA emulator. Considering the skin and proximity effects in the winding, the AC resistance of inductor is a frequency-dependent parameter. So, from the control design viewpoint, equivalent series resistance (ESR) of the inductor is an uncertain parameter. In this section, the effect of ESR changes on the stability of the closed-loop controller is studied.

Considering Figure 3, closed-loop transfer function of the system can be written as:

$$H(s) = \frac{y}{r} = \frac{\left(k_p + \frac{k_i}{s}\right)\frac{\frac{DX_2}{RC_{dc}}}{L_{dc}\left(s + \frac{D^2}{RC_{dc}}\right)\left(s + \frac{r}{L_{dc}}\right) + \frac{1}{C_{dc}}}}{1 + \left(k_p + \frac{k_i}{s}\right)\frac{\frac{DX_2}{RC_{dc}}}{L_{dc}\left(s + \frac{D^2}{RC_{dc}}\right)\left(s + \frac{r}{L_{dc}}\right) + \frac{1}{C_{dc}}}} \tag{11}$$

and the characteristic equation:

$$a_0 s^3 + a_1 s^2 + a_2 s + a_3 s = 0 \tag{12}$$

where:

$$a_0 = RC_{dc}L_{dc} \tag{13}$$

$$a_1 = \left(rRC_{dc} + D^2 L_{dc}\right) \tag{14}$$

$$a_2 = \left(r^2 D + R\right) \tag{15}$$

$$a_3 = DX_2 k_i \tag{16}$$

Considering inductor ESR changes, to investigate the stability of the closed-loop system, Routh-Hurwitz stability criterion can be employed. So, the Routh array for generic cubic polynomial in (12) can be arranged as:

$$
\begin{array}{ccc}
s^3 & a_0 & a_2 \\
s^2 & a_1 & a_3 \\
s^1 & \dfrac{a_1 a_2 - a_0 a_3}{a_1} & \\
s^0 & a_3 &
\end{array}
$$

Considering nominal values of the converter elements in Figure 1b and controller parameters ($k_p = 0$ and $k_i = 100$), stability criteria can be simplified as follows. It is assumed that $D = 0.5$ on the operating point of the converter.

$$1175r^3 + 5.875r^2 + 55255r - 2694 \geq 0 \tag{17}$$

where r is ESR of the input inductor.

To find the stable range of converter, $y = 1175r^3 + 5.875r^2 + 55255r - 2694$ is plotted in Figure 5. It is seen that y is zero for $r = 0.051\ \Omega$.
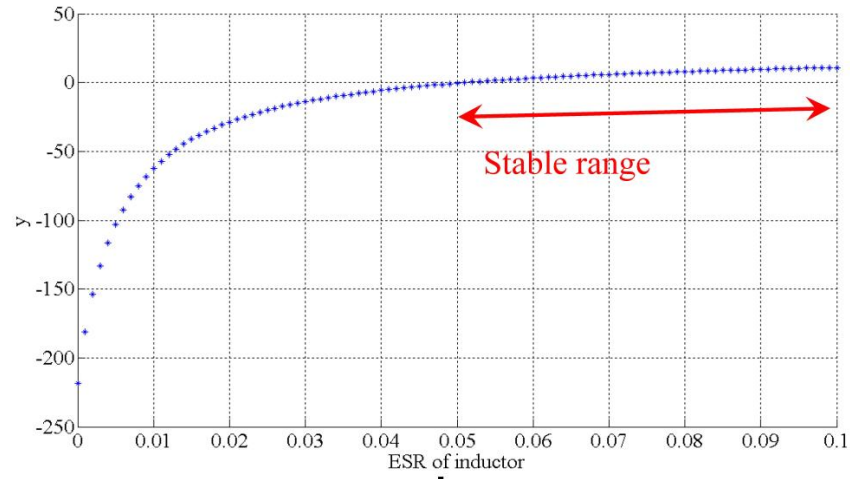
Figure 5. Stable operating range of the EMA emulator (y is output of the closed-loop system (inductor current)).

If it is assumed that if $r \ll 1$, then $\left(1175r^3 + 5.875r^2\right) \approx 0$. So, Equation (17) can be simplified as $55255r - 2694 \geq 0$, and the stable range of the closed-loop system will be $r \geq 0.0488\ \Omega$, which is compatible with zero crossing point of the characterize equation in Figure 5.

To investigate accuracy of the developed stability analysis, some simulations are done in MATLAB/Simulink. In Figure 6, the step responses of the designed linear controller for different values of the ESR are shown. The reference value of the EMA current is stepped up from 0 A to 6 A at t = 0.01 s. It is seen that, for $r = 0.04\ \Omega$, the response is unstable, which is compatible with the developed analysis. Additionally, for $r \geq 0.3$, oscillations are completely damped in the step response.
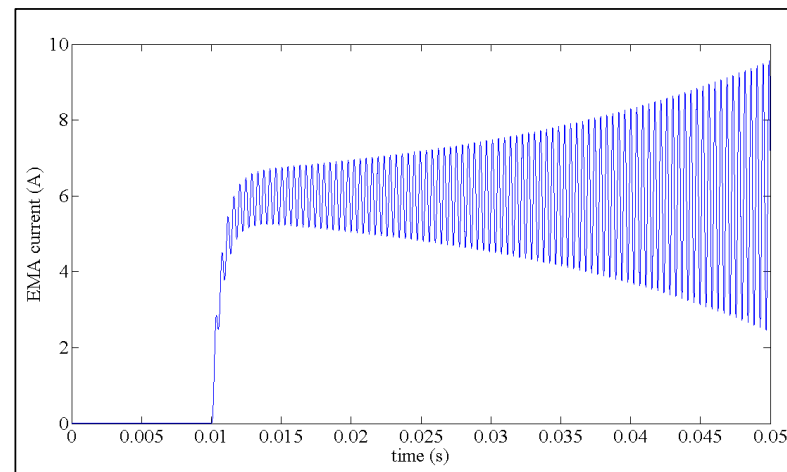
(a)

Figure 6. *Cont.*
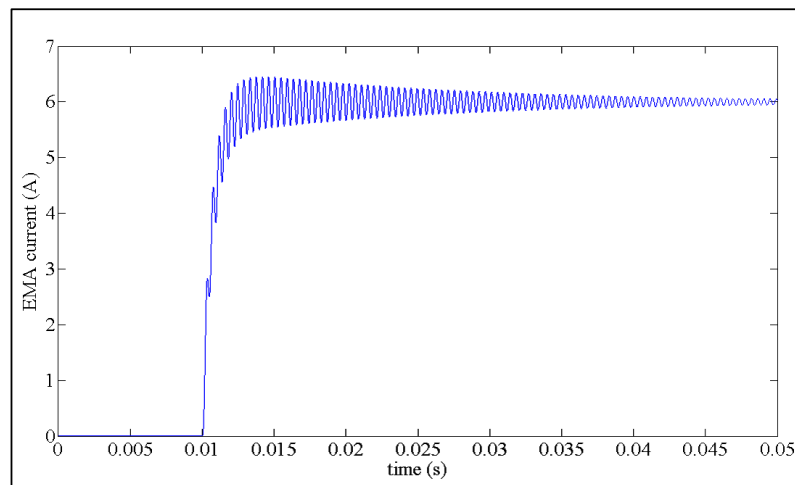
(**b**)
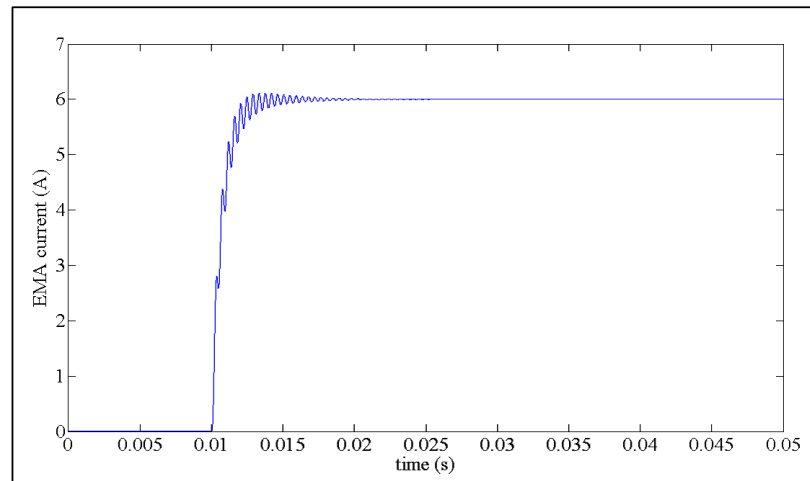
(**c**)
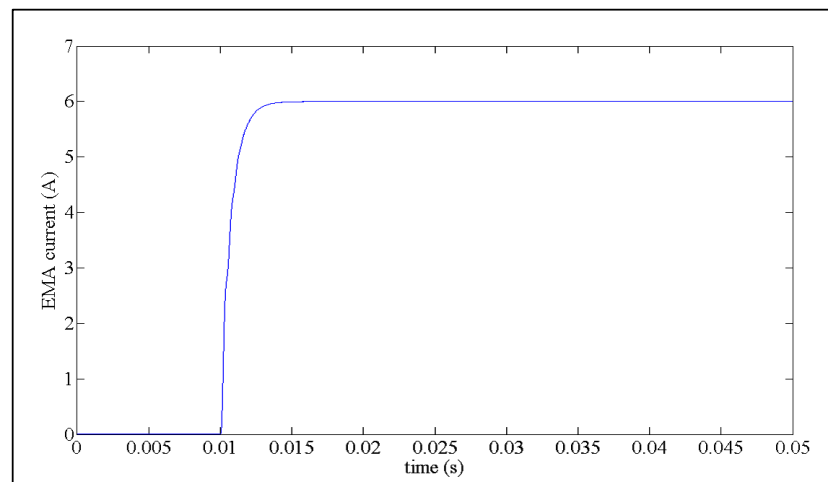
(**d**)

Figure 6. Step response of the closed-loop system for (**a**) $r = 0.04\ \Omega$, (**b**) $r = 0.06\ \Omega$, (**c**) $r = 0.09\ \Omega$, and (**d**) $r = 0.3\ \Omega$.

5. Dynamic Response Improvement

In this report, the linear current controller of the EMA converter is modified to improve the dynamic response of the closed-loop system. According to (8) and (9), the steady-state duty-cycle of the converter can be written as follows:

$$d = R\frac{X_{1s}}{X_{2s}} = \frac{RX_{1s}}{V_H - rX_{1s}} \tag{18}$$

Considering $V_H \gg rx_1$:

$$d \approx R\frac{x_1{}^*}{V_H} \tag{19}$$

where $x_1{}^*$ is reference of the input current.

Considering (19), in order to improve dynamic response of the system, a feed-forward loop can be added to the closed-loop controller, which is shown in Figure 7.
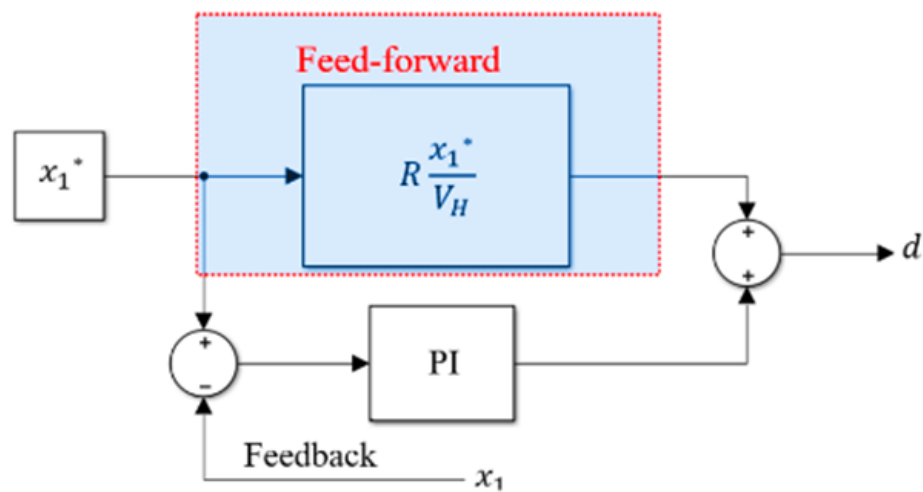
Figure 7. Modified linear controller.

To investigate the modified linear controller, the step response of the closed-loop system at different operating points is shown in Figure 8. It is seen that the rise/fall time of the response is around 150 μs, which is about 65 times faster than the conventional PI controller.
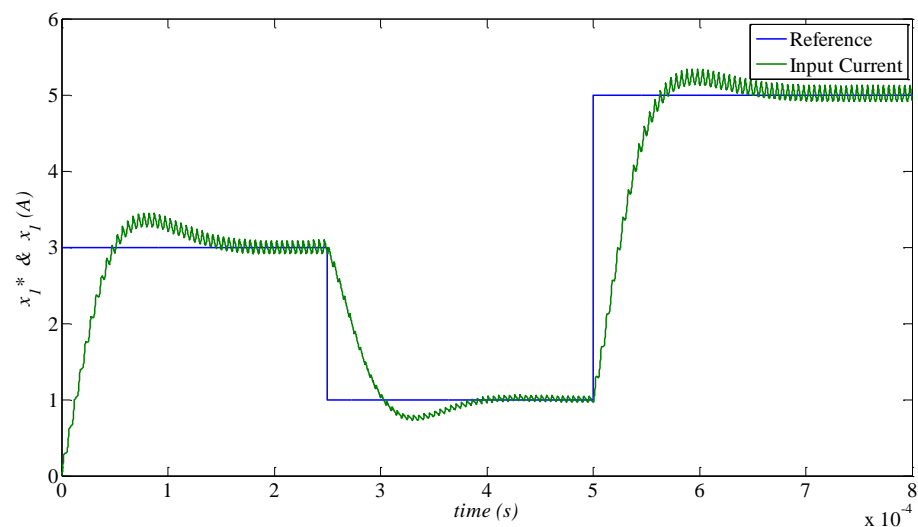
Figure 8. Step response of the improved linear controller.

6. Sliding Mode Controller Design for Input Current Control of the EMA Emulator

To improve the robustness of the closed-loop system against model uncertainties and disturbances, an SMC is developed for input current control of the EMA emulator. Despite the changes of converter operating point in a wide range, the SMC control is able to stabilize the closed-loop system satisfactorily.

At first, the equivalent SMC is designed according to certain nominal values of the model parameters. However, the uncertainties and required modifications for controller improvement will be studied in the next sections. Assuming the nominal values of the model parameters in Figure 1b, such as r_n, L_{dcn}, C_{dcn}, R_n, and V_{Hn} (n stands for the nominal value), to simplify the matrix representation of state-space model, the following parameters can be defined considering Equation (2):

$$\theta_{1n} = \frac{r_n}{L_{dcn}}, \ \theta_{2n} = \frac{1}{L_{dcn}}, \ \theta_{3n} = \frac{1}{C_{dcn}}, \ \theta_{4n} = \frac{1}{R_n C_{dcn}}, \ \theta_w = \frac{V_{Hn}}{L_{dcn}} \tag{20}$$

So, the averaged state-space model of the EMA converter in Equation (2) can be rewritten as follows, considering the nominal parameter.

$$\begin{pmatrix} \dot{x}_1 \\ \dot{x}_2 \end{pmatrix} = \begin{pmatrix} -\theta_{1n} & -\theta_{2n} \\ \theta_{3n} & -\theta_{4n}d^2 \end{pmatrix} \begin{pmatrix} x_1 \\ x_2 \end{pmatrix} + \begin{pmatrix} \theta_w \\ 0 \end{pmatrix} \tag{21}$$

To design the SMC, the error variables of the system can be defined as:

$$z_1 = x_1 - x_1{}^*, \ z_2 = x_2 - x_2{}^* \tag{22}$$

where $x_2{}^*$ is reference value of the capacitor voltage (x_2). According to (8) and (9), and assuming that $V_H \gg rx_1$, the reference of the capacitor voltage can be approximated as:

$$x_2{}^* \approx V_H \tag{23}$$

However, to eliminate steady-state error, Equation (23) can be rewritten as:

$$x_2{}^* = V_H + k_i \int z_1 dt \tag{24}$$

where k_i is a design parameter.

At first, nominal sliding surface is defined as:

$$S_n = z_2 \tag{25}$$

If it is assumed that the converter dynamics are settled on the sliding surface, then $S_n = 0$ is obtained. As a result, in sliding mode, time derivative of the sliding surface will be zero, as well. According to (24) and (25), the time-derivative of the sliding surface can be written as follows.

$$\dot{S}_n = -k_i z_1 + \dot{x}_2 \tag{26}$$

By replacing for $\dot{x}_2$ from (21) into (26):

$$\dot{S}_n = -k_i z_1 + \theta_{3n} x_1 - \theta_{4n} d x_2 \tag{27}$$

Considering the parameters nominal values, the equivalent SMC can be obtained by setting Equation (27) into zero.

$$d_{eq} = \frac{1}{\theta_{4n} x_2} (\theta_{3n} x_1 - k_i z_1) \tag{28}$$

By setting error variables into zero in Equation (28), the following equation can be obtained for steady-state operation, which is compatible with Equation (8):

$$D = \frac{1}{\theta_{4n}x_2}(\theta_{3n}x_1) = \frac{R_n x_1}{x_2} \tag{29}$$

7. Selection of the Sliding Mode Controller Gain

In this section, a selection of the SMC gain is studied. By replacing (28) in (21), the closed-loop model of the system can be obtained as follows:

$$\begin{pmatrix} \dot{x}_1 \\ \dot{x}_2 \end{pmatrix} = AX + B = \begin{pmatrix} -\theta_{1n} & -\theta_{2n} \\ k_i & 0 \end{pmatrix} \begin{pmatrix} x_1 \\ x_2 \end{pmatrix} + \begin{pmatrix} \theta_w \\ -k_i x_1{}^* \end{pmatrix} \tag{30}$$

Considering (30), it is seen that closed-loop behaviour of the EMA converter under the designed SMC is a linear model. So, in order to investigate its stability, a characteristic equation for the designed controller can be calculated by using $|sI - A| = 0$, where s is the Laplace operator.

$$s^2 + \frac{r_n}{L_{dcn}}s + \frac{k_i}{L_{dcn}} = 0 \tag{31}$$

Considering the nominal values of the converter parameters, r_n and L_{dcn} are always positive, so if $k_i > 0$ is selected, the roots of the system characteristic equation in (31) will always be in the left half-plane, and the stability of the closed-loop controller will be guaranteed for $k_i > 0$. Similar to previous linear controllers, $k_i = 100$ is selected for developed SMC as well.

8. Stability Analysis

Clearly, if the model parameters in (28) do not be equal to nominal values, then the proposed SMC in (28) cannot force the sliding surface and its time derivative into zero ($S_n \neq 0$ and $\dot{S}_n \neq 0$). So, in the presence of model uncertainty, the system response cannot be settled on the sliding surface. Hence, the developed equivalent SMC should be modified to achieve robust and stable behaviour from the closed-loop system. Considering model uncertainty, and according to Equation (27), the sliding surface derivative can be written as:

$$\dot{S} = \dot{S}_n + q = (-k_i z_1 + \theta_{3n}x_1 - \theta_{4n}dx_2) + q \tag{32}$$

where q is system uncertain compressed function and S_n is sliding surface of the nominal parameters. Clearly, on the sliding surface, $S = S_n = 0$. The system uncertainties are expressed by q in (32). To improve robustness of the designed controllers against model uncertainties, developed equivalent controller in (28) is revised as:

$$d = d_{eq} + \widetilde{d} = \frac{1}{\theta_{4n}x_2}(\theta_{3n}x_1 - k_i z_1 + k_C S + \hat{\rho} sgn(S)) \tag{33}$$

where d_{eq} is system equivalent controller for nominal parameters. Obviously, controller gains should be selected to satisfy $0 \leq d \leq 1$. Additionally, k_C is a positive scaler. In (33), $k_C S$ modifies the reaching path of the controller toward sliding surface. Moreover, $\hat{\rho}$ is an estimation from highest value of the uncertain compressed function q :

$$|q| < \hat{\rho} \tag{34}$$

Despite model uncertainties and load disturbances, it can be proved that the system response will certainly be on the sliding surface by using the modified controller in (33). To do so, $\dot{S}$ can be simplified by replacing (33) in (32).

$$\dot{S} = -[k_C S + \hat{\rho} sgn(S)] + q \tag{35}$$

If Lyapunov function is defined as:

$$V = \frac{1}{2}S^2 + \frac{1}{2}\tilde{\rho}^2 \qquad (36)$$

where $\tilde{\rho} = \hat{\rho} - \rho$, then time derivative of Lyapunov function will be:

$$\dot{V} = S\dot{S} + \tilde{\rho}\dot{\tilde{\rho}} \qquad (37)$$

By placing (35) in (37) and considering $\dot{\tilde{\rho}} = \dot{\hat{\rho}}$, the time derivative of Lyapunov function can be simplified:

$$\dot{V} = S\{-[k_C S + \hat{\rho}sgn(S)] + q\} + \dot{\hat{\rho}}(\hat{\rho} - \rho) \qquad (38)$$

Assuming $\dot{\hat{\rho}} = |S|$ and according to $S \times sgn(S) = |S|$, Equation (38) can be rewritten as:

$$\dot{V} = -k_C S^2 + qS - \rho|S| \qquad (39)$$

Considering Equation (34), it is clear that $qS \leq |q||S|$. Hence, the following equation can be written according to (39):

$$\dot{V} \leq -k_C S^2 + |S|(|q| - \hat{\rho}) \qquad (40)$$

As $(-k_C S^2) \leq 0$ and $|q| < \rho$, the time derivative of the Lyapunov function in (40) will be a negative semi-definite function. So, the asymptotical stability of the system will be proved using modified SMC in (33) and $\dot{\hat{\rho}} = |S|$ as an estimation law.

9. Proposed SMC for EMA Emulator

To improve robustness of the system, in the previous section, the SMC controller has been modified. Additionally, an estimation law has been extracted for the proposed SMC. To cope with the model uncertainties, another approach for the modification of the equivalent SMC is presented:

$$d = d_{eq} + \tilde{d} = \frac{1}{\theta_{4n}x_2}(\theta_{3n}x_1 - k_i z_1 + \rho sgn(S)) \qquad (41)$$

If Equation (41) is employed as a SMC, despite system uncertainties, the asymptotical stability of the proposed controller can be proved by choosing $\rho > |q|$. In this condition, the previous estimation rule will not be needed anymore.

By replacing (41) into (32):

$$\dot{S} = \dot{S}_n + q = -\rho sgn(S) + q \qquad (42)$$

If Lyapunov function and its time derivative are assumed as:

$$V = \frac{1}{2}S^2 \rightarrow \dot{V} = S\dot{S} \qquad (43)$$

By replacing $\dot{S}$ from (42) in (43):

$$\dot{V} = S(-\rho sgn(S) + q) = -\rho|S| + qS \qquad (44)$$

Considering $qS \leq |q||S|$, Equation (44) can be simplified as:

$$\dot{V} = -\rho|S| + qS \leq -\rho|S| + |q||S| \qquad (45)$$

As ρ is selected to be more than the uncertainty function ($\rho > |q|$):

$$\dot{V} \leq |S|(-\rho + |q|) \leq 0 \tag{46}$$

Hence, despite the presence of model uncertainness and load change in the EMA emulator, it is observed that $\dot{V}$ is a negative semi-definite function in (46), and as a result, asymptotical stability of the controller presented in (41) will be proven. Considering Equation (41), the block diagram of the implemented SMC is shown in Figure 9.
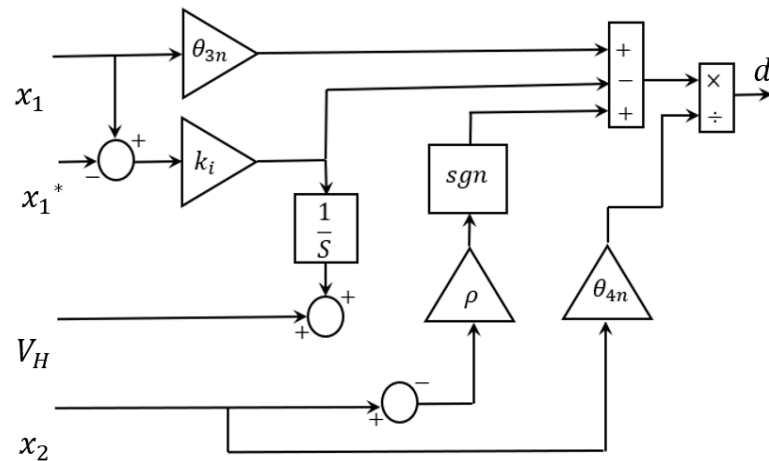
Figure 9. Block diagram of the implemented SMC regarding the Equation (41).

In Figure 10, step response of the designed SMC in (41) is illustrated in similar condition with the previous simulations. It is seen that the rise/fall time of the inductor current is about 100 μs.
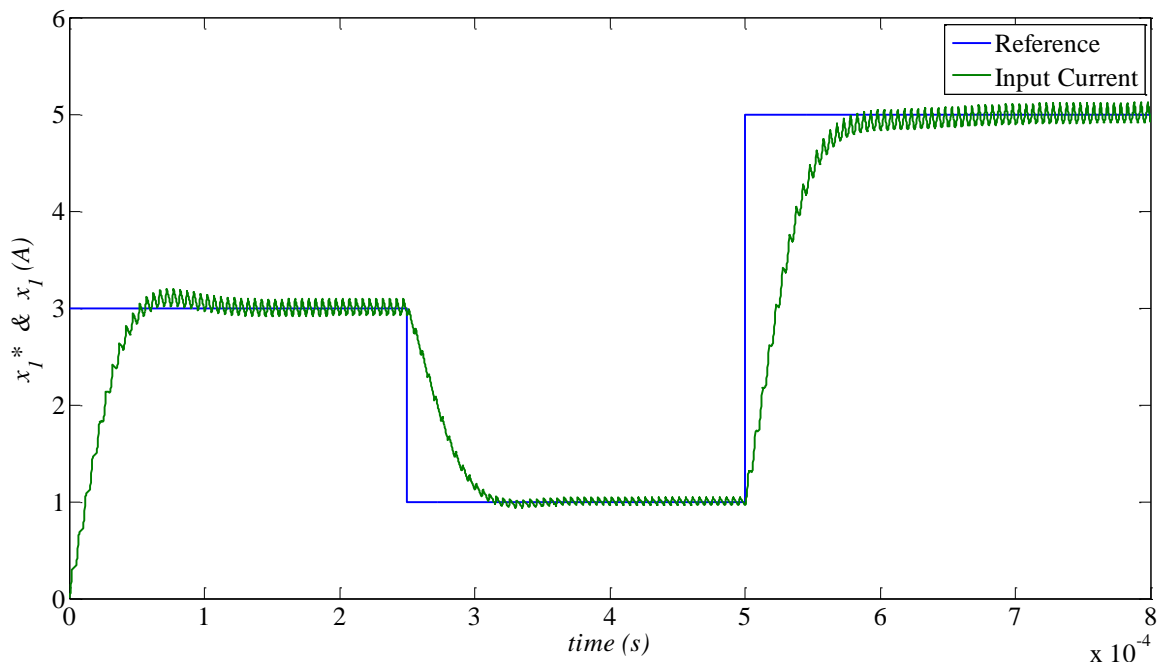
Figure 10. Step response of the proposed SMC.

10. Comparison of the Modified Linear Controller and SMC

In this section, the dynamic responses of the modified linear controller are compared with the developed SMC in (41).

10.1. Load Changes

As load resistance is an uncertain parameter, the response of the proposed controllers should be studied for different load values. In this test, it was assumed that the load resistance had 10% tolerance, and $R = 25.85 \, \Omega$ was used in the simulation. The nominal value of the load resistance was $R = 23.5 \, \Omega$. It was seen that the proposed SMC had better dynamic response against the uncertainty of the load value in Figure 11.
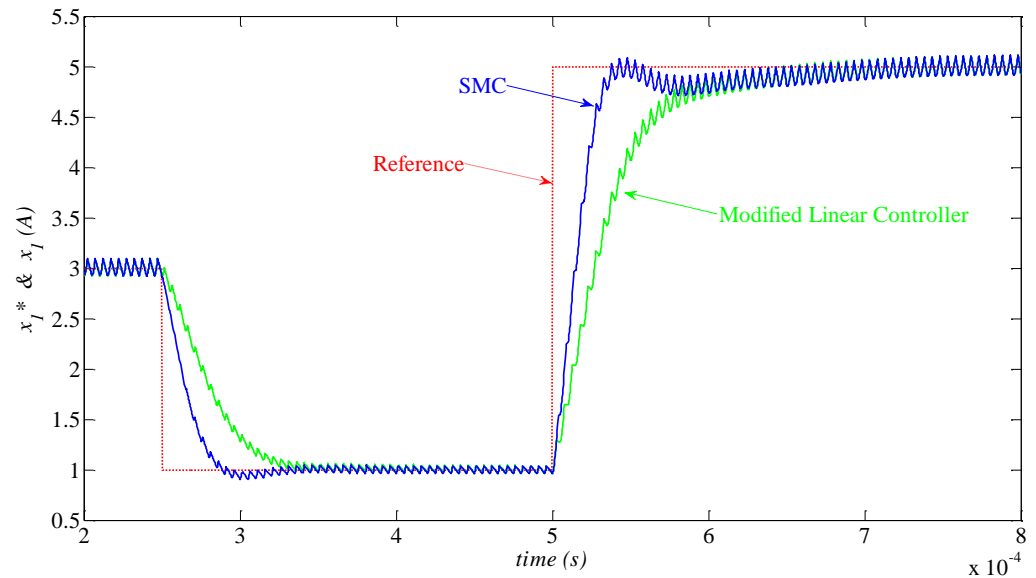
Figure 11. Step response of the proposed controllers considering load uncertainty.

10.2. Changes of Inductor's ESR

The equivalent series resistance (r) of the inductor is another uncertain parameter in the EMA emulator. During the controller design in the previous sections, it was assumed that $r = 0.25 \, \Omega$, and the gains of the controllers were selected to have acceptable transient and dynamic responses. However, the robustness of the designed controllers should be investigated during the changes of the parasitic resistor. In Figure 12, it is assumed that $r = 1.3 \, \Omega$, and the step responses of the SMC and modified linear controller are compared.
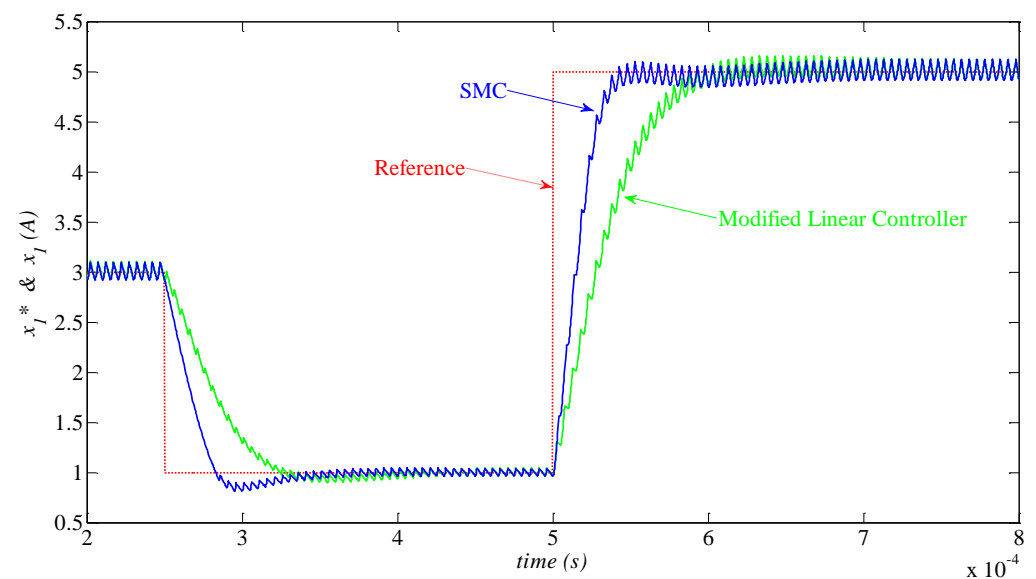
Figure 12. Step response of the developed controllers considering inductor's ESR uncertainty.

11. Experimental Validation

11.1. Experimental Setup

The experimental work on EMA emulator presented in this paper was part of a larger project that aimed at developing a system to interface supercapacitor energy storage to the 270 V power bus for smoothing the power absorbed by an EMA. In order to achieve high power density a high efficiency converter interface, the use of GaN power switches was developed that could be jointly used also in the EMA emulator. The nominal values of the converter parameters are shown in Table 2.

Table 2. Nominal values of the parameters in the EMA emulator.

Parameter	Description	Value
V_H	Input voltage of the converter	270 V
r	Equivalent series resistance of the inductor	0.25 Ω
L_{dc}	Input inductor	47 μH
C_{dc}	DC link capacitor	100 μF
R	Load resistance	23.5 Ω

The 650 V—13 mΩ enhancement mode HEMT GaN Half-Bridge (GSP65R13HB-EVB) converter from *GaN-Systems* was employed to achieve high efficiency with acceptable power density. To reduce the size of the magnetics in the LC filters, the switching frequency was set at 200 kHz. Additionally, for safe operation, a dead time of 100 ns was used when turning on the complementary switches of the half bridge inverter. The cooling was performed by a fan mounted on the heatsink of the GaN switches. The laboratory test rig, built for the performance evaluation of the developed controller, is shown in Figure 13. The LAH-25-VP LEM, which has an appropriate bandwidth on 200 kHz, was employed as a Hall effect current sensor for measurement of the input current feedback signal. Additionally, a TELEDYNE LECROY 1MHz current probe was used for monitoring of the current signals. The Teledyne LeCroy HDO4024A Bench Digital Storage Oscilloscope, 200 MHz, 4 Channels, was used. For the practical verification of the proposed controller structure, the TMS320F28335PGFA DSP from Texas Instrument was used for implementation by programming it in Code-Composer Studio 6.0.1 software. A moving average technique was employed for smoothing of the current samples of the feedback signals in the DSP program. Analogue signals are read in an interrupt service routine with 20 kHz sampling frequency.

To improve the noise immunity of the system, the fibre optic communication of the PWM signals between the DSP and converter board was employed. In this condition, an about 1.2 microsecond delay was seen in the gate switching signals from the DSP board to the converter motherboard. However, it did not affect the steady state error of the converter, due to presence of an appropriate feedback loop.

11.2. Experimental Results

11.2.1. Steady-State Operation

Response of the proposed SMC in steady-state operation is shown in Figure 14. In this test, the reference of the input current was $x_1{}^* = 5$ A. It was seen that the controller could stabilize the EMA converter with zero steady-state error. In this condition, the input power was equal to 1350 W. Considering the nominal power of the converter, a wire-wound-type, resistor which has a considerable parasitic inductance, was employed as a load. Hence, the current ripple of the load was about 8 A pk-pk. From the controller design viewpoint, the current ripple can be assumed as a load disturbance. However, despite the presence of large disturbances, the SMC was able to reject it properly and stabilize the EMA current satisfactorily.
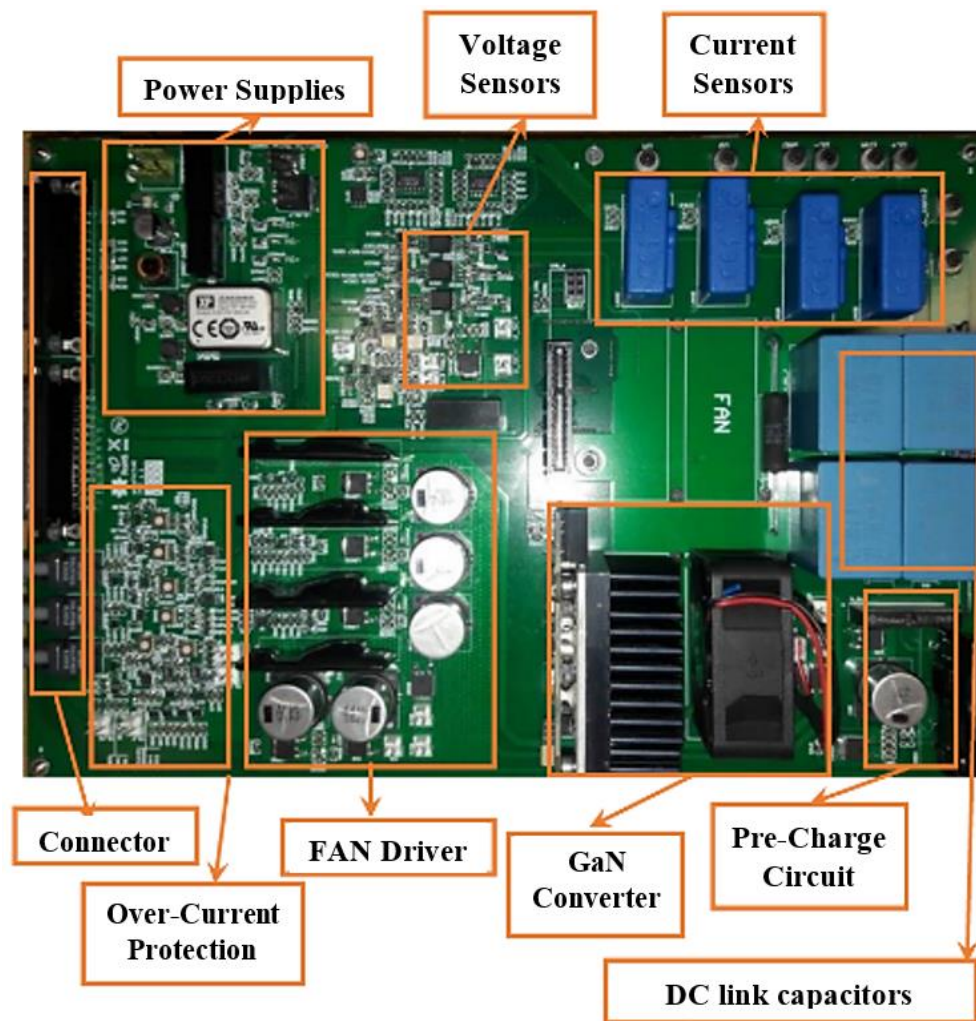
(**a**)
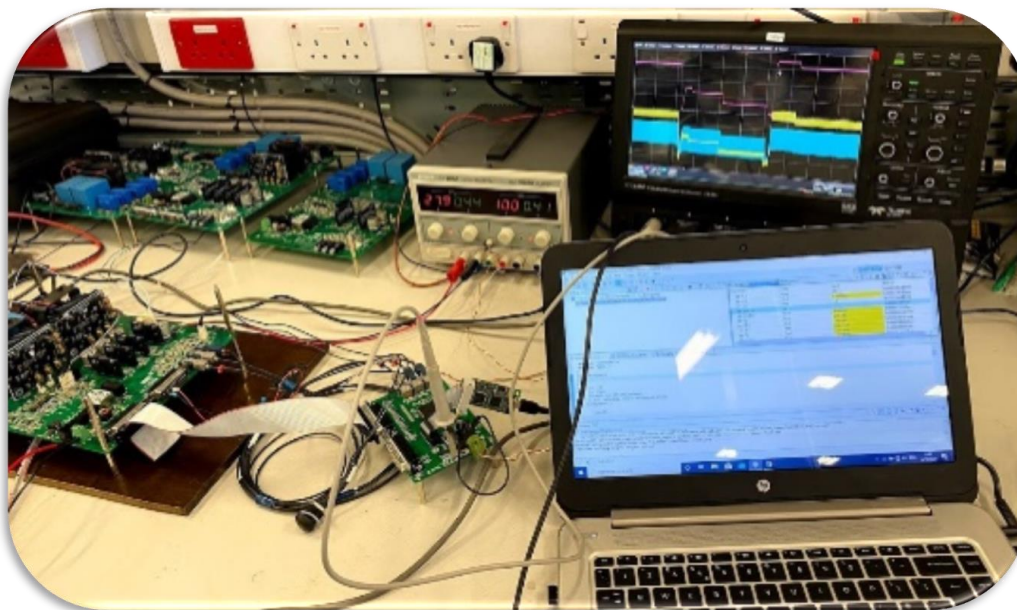
(**b**)

Figure 13. Experimental setup for performance evaluation of the proposed SMC; (**a**) Designed converter. (**b**) Experimental rig.
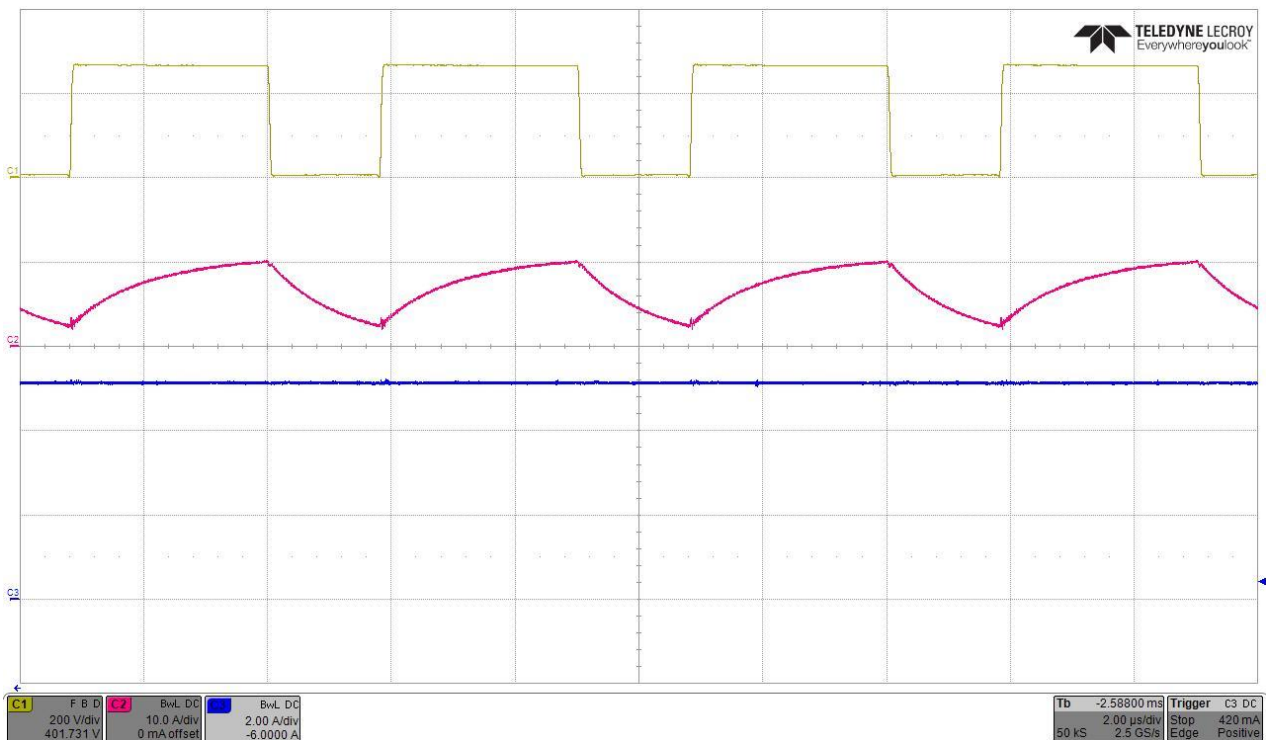
Figure 14. Response of the proposed SMC in steady-state operation (load voltage (yellow), load current (purple), and input/EMA current (blue)).

11.2.2. Step Changes of the Reference Current

At first, the response of the SMC was illustrated during controller start-up. It is assumed that reference value of the input current stepped from 0 A to 5 A, and the load voltage, load current, and input current are shown in Figure 15. It was seen that the time rise time of the controller response was about 330 microseconds. Despite the presence of a large current ripple, it was observed that the response of the designed SMC was robust and stable in a wide range of input current change.
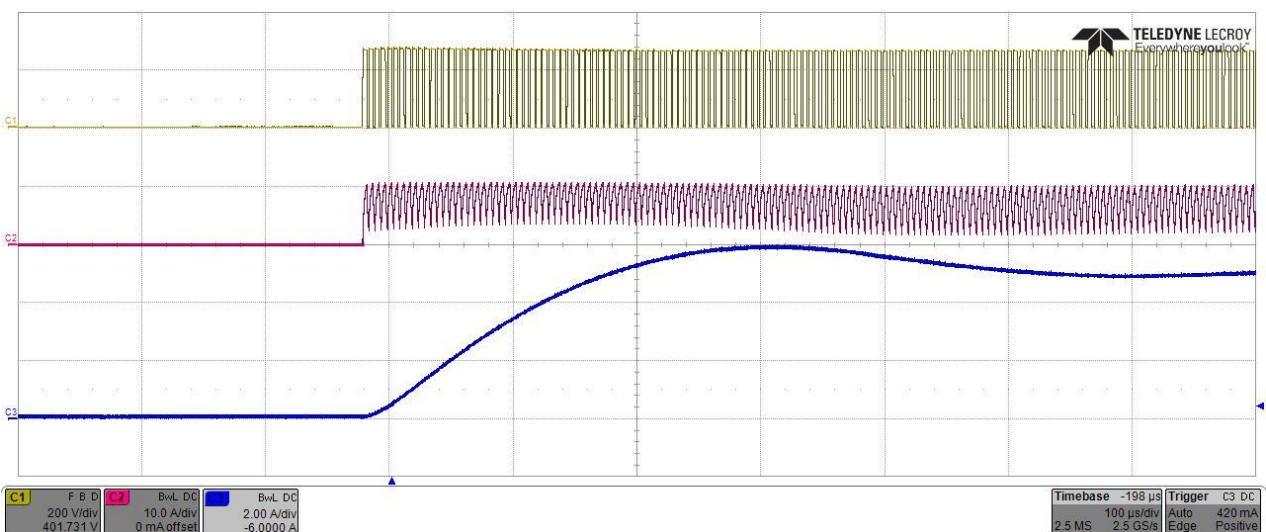
Figure 15. Response of the proposed SMC during controller start-up (load voltage (yellow), load current (purple), and input/EMA current (blue)).

Additionally, in Figure 16, it is assumed that reference current of the EMA converter stepped up from 0 A to 4 A, and then it stepped down from 4 A to 0 A. It is seen that the controller can track the reference value with zero steady-state error.
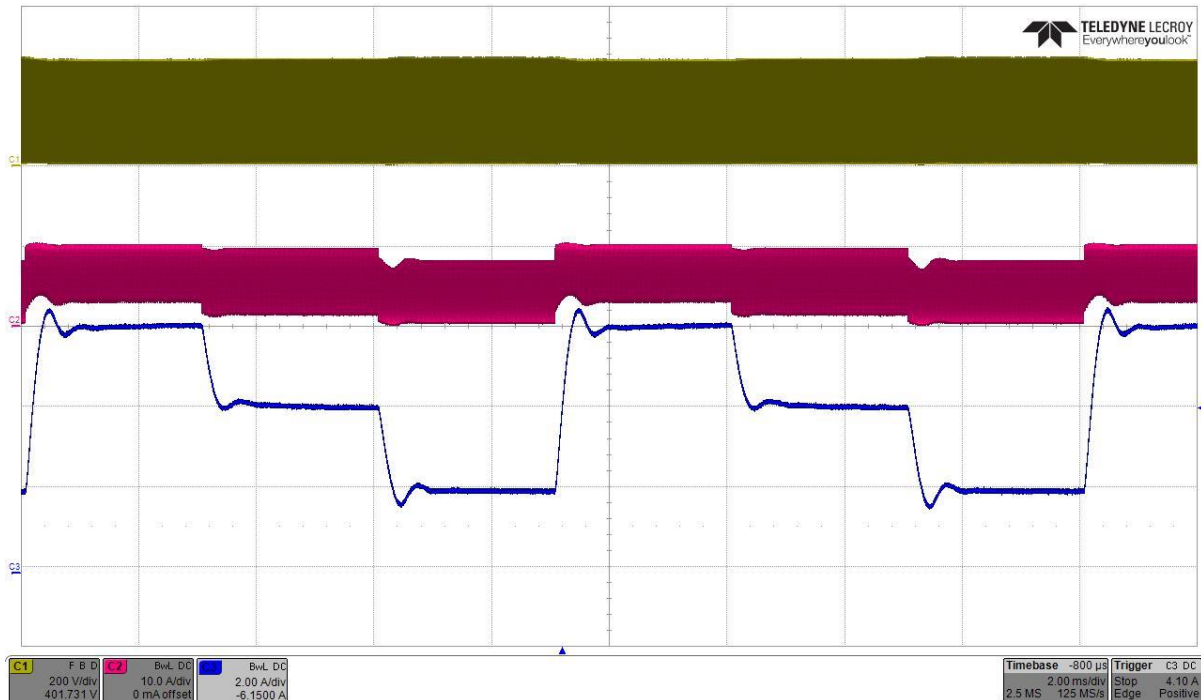
Figure 16. Response of the proposed SMC during step changes of the input current from 0 A to 6 A and from 6 A to 4 A and 2 A. (load voltage (yellow), load current (purple) and input/EMA current (blue)).

Finally, Figure 17 shows the response of the proposed SMC when evaluating the performance of the designed closed-loop system when producing the typical Dc bus current profile of an EMA, as defined in Figure 1. In this test, the reference current profile of the converter was similar to a real EMA, Figure 1a. Regarding the previous results, in this test, the load current has considerable current ripple. However, the proposed SMC can stabilize the input current of the converter robustly on different reference levels with acceptable steady-state and dynamic responses.
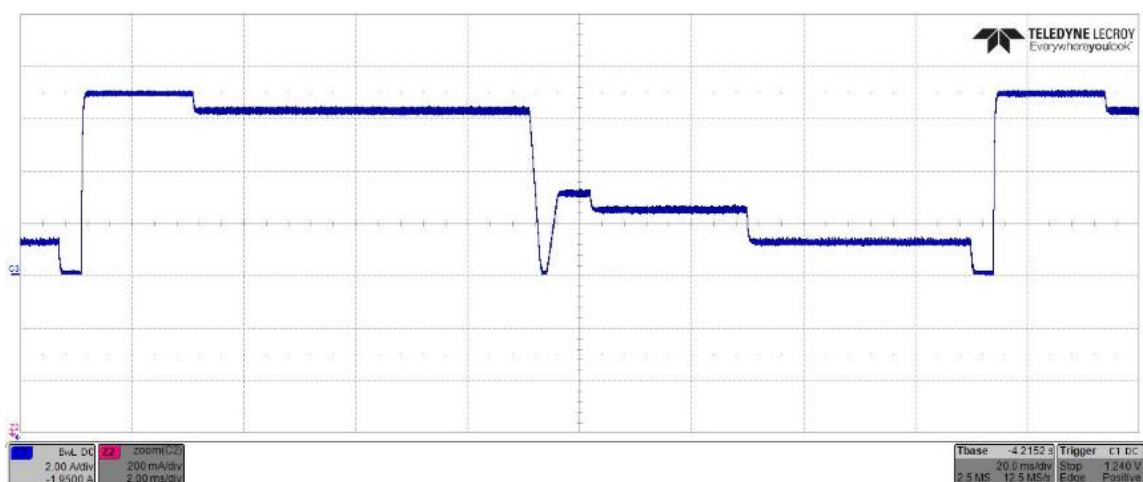
Figure 17. Response of the proposed SMC during step changes of the input current reference in a wide range of operation for a real EMA power profile.

12. Conclusions

In this paper, the closed-loop control of the EMA emulator was studied using GaN based synchronous DC-DC buck converters. Due to the inherent challenges of controller design, e.g., the model nonlinearity, changes of the operating point in a wide range, and resonance issues of the input LC filter, it was shown that the linear PI-feedforward controller could not stabilize the closed-loop system against the model uncertainties. Hence, to cope with the mentioned issue, a novel fixed frequency SMC was developed for closed-loop stabilization of the EMA emulator. Using the Lyapunov stability criteria, the asymptotic stability of the developed controller was proven in the whole operational range of system, and it was proven that the SMC can reject the external disturbances, resonance issues of the LC input filter, and model uncertainties stably. The proposed nonlinear SMC controller enjoys a very simple control law. Hence, despite having very high switching and sampling frequencies, it can be easily implemented. The experimental response of the designed synchronous DC-DC buck converter was evaluated experimentally by implementing the control strategy in a TMS320F28335PGFA DSP from *Texas Instrument*. Moreover, the comprehensive comparison of the proposed SMC controller and a PI-feedforward controller proved the superior performance of the developed closed-loop system, in terms of the transient time response, robustness, and stability of the EMA emulator.

References

1. Sarlioglu, B.; Morris, C.T. More Electric Aircraft: Review, Challenges, and Opportunities for Commercial Transport Aircraft. *IEEE Trans. Transp. Electrif.* **2015**, *1*, 54–64. [CrossRef]
2. Keshmiri, N.; Wang, D.; Agrawal, B.; Hou, R.; Emadi, A. Current Status and Future Trends of GaN HEMTs in Electrified Transportation. *IEEE Access* **2020**, *8*, 70553–70571. [CrossRef]
3. Cao, Z.; Zhou, Y.; Sun, L.; Liu, L. Multi-resolution modeling based on structure in application of more electric aircraft EMA system. In Proceedings of the 2017 International Conference on Circuits, Devices and Systems (ICCDS), Chengdu, China, 5–8 September 2017; pp. 106–109. [CrossRef]
4. Trentin, A.; Zanchetta, P.; Wheeler, P.; Clare, J. Power flow analysis in electro-mechanical actuators for civil aircraft. *IET Electr. Power Appl.* **2011**, *5*, 48–58. [CrossRef]
5. Jiang, W.; Chincholkar, S.H.; Chan, C. Investigation of a Voltage-Mode Controller for a dc-dc Multilevel Boost Converter. *IEEE Trans. Circuits Syst. II Express Briefs* **2018**, *65*, 908–912. [CrossRef]
6. Moraka, O.J.; Barendse, P.S.; Khan, M.A. Dead Time Effect on the Double-Loop Control Strategy for a Boost Inverter. *IEEE Trans. Ind. Appl.* **2017**, *53*, 319–326. [CrossRef]
7. Cui, M.; Sun, R.; Bu, Q.; Liu, W.; Wen, H.; Li, A.; Liang, Y.C.; Zhao, C. Monolithic GaN Half-Bridge Stages With Integrated Gate Drivers for High Temperature DC-DC Buck Converters. *IEEE Access* **2019**, *7*, 184375–184384. [CrossRef]
8. Venkatramanan, D.; John, V. Dynamic Modeling and Analysis of Buck Converter Based Solar PV Charge Controller for Improved MPPT Performance. *IEEE Trans. Ind. Appl.* **2019**, *55*, 6234–6246. [CrossRef]
9. Pang, S.; Nahid-Mobarakeh, B.; Pierfederici, S.; Huangfu, Y.; Luo, G.; Gao, F. Large-Signal Stable Nonlinear Control of DC/DC Power Converter With Online Estimation of Uncertainties. *IEEE J. Emerg. Sel. Top. Power Electron.* **2021**, *9*, 7355–7368. [CrossRef]
10. Saadat, S.A.; Ghamari, S.M.; Mollaee, H. Adaptive backstepping controller design on Buck converter with a novel improved identification method. *IET Control Theory Appl.* **2022**, *16*, 485–495. [CrossRef]
11. Li, X.; Li, Y.; Seem, J.E. Maximum Power Point Tracking for Photovoltaic System Using Adaptive Extremum Seeking Control. *IEEE Trans. Control Syst. Technol.* **2013**, *21*, 2315–2322. [CrossRef]

12.	Repecho, V.; Biel, D.; Ramos-Lara, R.; Vega, P.G. Fixed-Switching Frequency Interleaved Sliding Mode Eight-Phase Synchronous Buck Converter. *IEEE Trans. Power Electron.* **2018**, *33*, 676–688. [CrossRef]

13.	Pang, S.; Hashjin, S.A.; Nahid-Mobarakeh, B.; Pierfederici, S.; Huangfu, Y.; Luo, G.; Gao, F. Large-Signal Stabilization of Power Converters Cascaded Input Filter Using Adaptive Energy Shaping Control. *IEEE Trans. Transp. Electrif.* **2021**, *7*, 838–853. [CrossRef]